Carbon 133 (2018) 267–274

Contents lists available at ScienceDirect

Carbon

journal homepage: www.elsevier.com/locate/carbon

Atomistic insights into the effect of polymerization on the thermophysical properties of 2-D C_{60} molecular solids

Abduljabar Qassem Alsayoud [a, b], Venkateswara Rao Manga [a], Krishna Muralidharan [a, c, *], Joshua Vita [a], Stefan Bringuier [a], Keith Runge [a], Pierre Deymier [a]

[a] Department of Materials Science and Engineering, University of Arizona, Tucson, AZ 85721, USA
[b] Department of Mechanical Engineering, King Fahd University of Petroleum & Minerals (KFUPM), Dhahran 31261, Saudi Arabia
[c] Lunar and Planetary Laboratory, University of Arizona, Tucson, AZ 85721, USA

ARTICLE INFO

Article history:
Received 3 January 2018
Accepted 11 January 2018
Available online 21 March 2018

ABSTRACT

The ability to polymerize solid-state C_{60} molecular crystals via intermolecular covalent bond formation provides controllable routes to obtaining structures with tunable mechanical and thermal properties. In this regard, using molecular dynamics simulations, fundamental insights into the interplay between degree of polymerization and the ensuing evolution in the thermophysical properties of C_{60} polymorphs are obtained for the first time. In particular, it is unambiguously shown that 2-D polymerized C_{60} polymorphs show a two order of magnitude enhancement in the thermal conductivity and one order of magnitude change in the elastic stiffness. The significant increase in the thermal conductivity is correlated to the presence of new THz thermal phonon modes, characterized by larger mean free paths. In addition, it is also seen that the Debye temperature of the C_{60} structures is strongly dependent on the extent of polymerization. The new understanding obtained in this work provides valuable guidelines for the design and development of new C_{60} based phononic metamaterials for applications as vibrational and thermal management systems.

1. Introduction

Spherical fullerene molecules such as C_{60} exhibit interesting chemical properties due to their curvature and icosahedral symmetry [1]. Consequently, C_{60}, an electron acceptor, readily undergoes a variety of addition, cycloaddition and polymerization reactions [2]. In its solid state form, C_{60} forms an FCC molecular crystal at room temperature, which polymerizes by formation of covalent bonds between neighboring C_{60} molecules, when subjected to pressure, electric field or radiation [2–5]. Interestingly, the degree of polymerization (1-D vs. 2-D vs. 3-D) is tunable, depending on the nature and intensity of the external stimulus. In addition, recent advances in solution based crystal engineering have resulted in obtaining solvent-intercalated crystalline C_{60} self-assemblies that demonstrate chemistry-driven tunable polymerization [6] While the structural characteristics of the C_{60} polymers have been reasonably well studied [7], fundamental characterization of the thermophysical properties as a function of polymerization have not yet been systematically examined due to inherent difficulties in synthesizing pure phases. In this context, we carry out a detailed investigation on the interplay between polymerization and the resulting thermophysical properties using state of the art atomistic computational techniques. Given that the covalent bonding between C_{60} molecules should enable significant differences in the phonon derived properties of polymerized vs unpolymerized C_{60} polymorphs, special attention is paid to understand the changes in thermal phonon properties and the consequent effects on the variations in specific heat, Debye temperature, and thermal transport of the corresponding 2-D polymeric C_{60} structures. Lessons learned from this study will not only provide scientific insights into the interplay between extent of the polymerization and thermophysical properties, but with equal importance, provide fresh perspectives towards utilizing polymerized C_{60} structures for targeted thermal management applications.

* Corresponding author. Department of Materials Science and Engineering, University of Arizona, Tucson, AZ 85721, USA.
E-mail addresses: alsayoud@email.arizona.edu (A.Q. Alsayoud), krishna@email.arizona.edu (K. Muralidharan).

https://doi.org/10.1016/j.carbon.2018.01.044
0008-6223/

2. Background

The most stable solid state C_{60} phase at ambient conditions is the unpolymerized FCC phase ($\alpha = 14.04$ *A*), while, the primary undoped polymeric C_{60} phases crystallize in either rhombahedral (R-phase) or tetragonal (T-phase) or orthorhombic (O-phase) structures. In the polymeric phases, the intermolecular bonding arises due to [2 + 2]-cycloaddition reactions [8] and is characterized by charge transfer between carbon double bonds in neighboring 6-fold C_{60} faces. In the absence of electric and optical stimulus, C_{60} polymerization requires both thermal and pressure activation, to ensure appropriate intermolecular orientation and separation. The O-phase consists of 1-D parallel chains of covalently bonded C_{60} molecules, while, both T-phase and R-phase consist of 2-D planes of covalently bonded C_{60} molecules as shown in Fig. 1. For the T-phase, each molecule is bonded to four nearest neighbors molecules ($\alpha = 9.09$ A, $c = 14.95$ A), while in the R-phase, each molecule is bonded to six nearest neighbors ($\alpha = 9.19$ A, $c = 24.5$ A).

Understanding the vibrational spectra of both unpolymerized and polymerized phases is necessary to enable a fundamental characterization of the respective phonon derived thermophysical properties. An important interrelationship between the different thermophysical properties is given in Eqn. (1) [9], linking the mode-by-mode contributions to the thermal conductivity (κ) of the material. For a given phonon frequency ω, υ_g, υ_p, c_υ, τ_r represent mode specific group velocity, phase velocity, heat capacity and life-time respectively, while $\omega_{L,max}$, $\omega_{T,max}$ represent the maximum longitudinal and transverse frequency that can be supported by the system. However, at high temperatures (relative to the Debye temperature) this equation is effectively reduced to Eqn. (2) [10], where C_V^ρ is the volumetric heat capacity, v_s represents the longitudinal speed of sound and λ is the effective mean free path of thermal phonons.

$$k = \frac{1}{6\pi^2}\left[\int_0^{\omega_{L,max}} \left(c_\upsilon \frac{\upsilon_g}{\upsilon_p^2}\tau_r\right)_L \omega^2 d\omega + 2\int_0^{\omega_{T,max}} \left(c_\upsilon \frac{\upsilon_g}{\upsilon_p^2}\tau_r\right)_T \omega^2 d\omega\right] \quad (1)$$

$$k = \frac{1}{3} C_V^\rho \upsilon_g \lambda \quad (2)$$

Past investigations have examined the vibrational properties of the FCC and the polymerized phases [9–15]. However, difficulties in producing pure phase polymerized structures and the sensitivity of C_{60} solids towards photo-polymerization introduce inherent uncertainties in the characterization of the C_{60} solids' vibrational properties. Based on available literature, the vibrational spectrum of the FCC phase can be characterized in terms of isolated intramolecular C_{60} peaks (8–60 *THz*) as well as additional lattice (intermolecular) modes up to 1.8 *THz*. For the polymerized phases, the underlying C_{60} symmetry is broken due to polymerization, lifting the degeneracy of some high symmetry intramolecular modes; in addition, new vibrational modes attributed to the covalent intermolecular bonds also arise, as discussed in Ref. [15].

In terms of thermophysical properties, the specific heat (C_V) and Debye temperature (θ_D) of the FCC molecular crystal have been studied in more detail as compared to the polymerized phases [16–18]. There is considerable scatter in the reported values of the Debye temperature of the FCC phase (θ_D~ 37–100 K) as shown in Ref. [19], while the thermal conductivity (κ~ 0.4 W/m-K) [16] has not been extensively studied. The low θ_D and κ of the FCC phase are a consequence of the weak intermolecular interactions between non-bonded C_{60} molecules. In addition, the reported values of C_V at 300 K for the FCC phase ranges between 490–740 mJ/g/K [19]. Literature on the thermophysical properties of the polymerized phases is relatively sparse [20–24] and often uncertain as pointed out before. For example, based on available literature, the θ_D for the 2-D polymerized phases is estimated to be anywhere between 42 K [24] to 215 K [20]. Further, thermal conductivity studies on the polymerized phases have been largely inconclusive due to large structural disorder associated with the synthesized polymeric structures [25–28].

As evident from this discussion, given the dearth of information on the polymerized C_{60} phases and considerable scatter in available literature associated with all three phases, there is a clear need for investigations to examine and characterize their thermophysical properties. Towards this end, using molecular dynamics (MD) simulations, the thermophysical properties of the molecular crystal FCC phase will be compared and contrasted with 2-D polymerized T-phase and R-phase structures, leading to insights that underlie key differences in their respective behaviors. For these purposes, a new interatomic potential, capable of modeling the above phases is specifically developed. Atomistic computational methods provide reliable means of obtaining a fundamental characterization of structure-property relations of materials, without resorting to more expensive experimental characterization techniques. Further, key insights obtained from such methods can provide important guidelines for design and synthesis of appropriate C_{60} structures for targeted technological applications.

In the next section, we provide details on the computational methods adopted in this work.

3. Models and methods

Quantum chemical methods such as density functional theory (DFT) have been utilized to examine the ground-state electronic properties of the FCC phase [29]. However, careful implementation

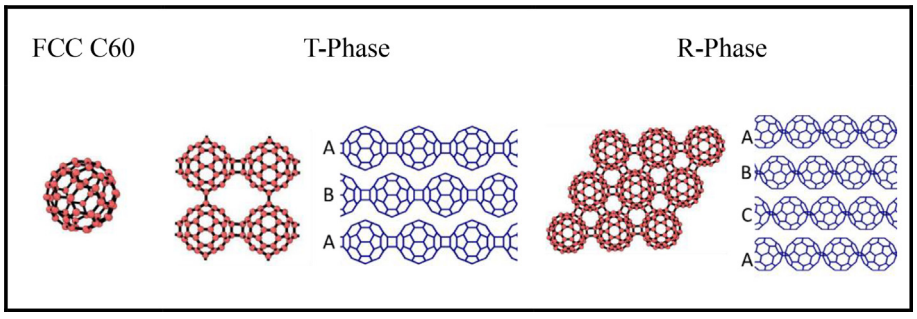

Fig. 1. Structures of FCC, T-Phase and R-Phase (Top and side view). (A colour version of this figure can be viewed online.)

of such methods have to be undertaken to include thermal effects to ensure accurate representation of the structure and thermophysical properties of the solid-state C_{60} polymorphs. Specifically, the FCC molecular solid is stabilized at temperatures greater than 260 K due to the rotation of the C_{60} molecules, which is temperature activated. The complete rotation of the C_{60} molecule renders them to be effectively spherically symmetric due to continuous reorientation, allowing the molecular solid-phase to be treated as an FCC structure. Thus, in principle, DFT examinations of the FCC structure as well as other polymorphs should include different relative configurations of neighboring C_{60} molecules, necessitating the need for large supercells. Further, properties such as thermal conductivity require the ability to include temperature dependent anharmonic effects for accurate representation of phonon scattering processes. Towards this end, third (and higher-order) derivatives of the dynamical matrix obtained from 0 K DFT calculations are used in conjunction with a linearized Boltzmann Transport Equation (BTE) framework. Given the complexity in evaluating higher-order derivatives, typical DFT-BTE implementations only utilize third-order derivatives, and are thereby restricted to considering three phonon scattering processes [30].

In this regard, classical molecular dynamics (MD) simulations provide a welcome compromise, if appropriate interatomic potentials are chosen. In particular, they allow for conducting finite temperature simulations of larger ensembles, where different structural configurations can be sampled effectively. Further, temperature driven phonon anharmonicity can be explicitly captured, providing the ability to accurately examine the different thermophysical properties. In this context, the choice of the potential as well as the adopted methods to evaluate the thermophysical properties is discussed below.

3.1. Interatomic potential models

To model the FCC phase, the potential should be capable of representing intramolecular sp^2 bonding as well as longer range van der Waal interactions, while for the polymerized phases, additional sp^3 bonding has to be accounted for. A preliminary test of available potentials was conducted, which included Tersoff [31], LCBOP, and Airebo [32,33] force-fields. However, none of these potentials were able to stabilize the room temperature T-phase and R-phase over extended MD-simulation timescales (~ns). Thus, in this work, the Tersoff potential (Eqn. (3)) as parameterized in Ref. [31] was used to simulate the bonded interactions (sp^2, sp^3), while the van der Waals interactions were simulated using a Morse potential (Eqn. (4)), which was fitted to the long-range part of the LCBOP potential [33]. Note that the long-range potential was restricted to interactions between atoms belonging to different molecules; if neighboring molecules were bonded (as is the case in polymerized structures), then the van der Waal interactions were turned off. The functional form of the potential is given in Eqn. (4) and the corresponding parameters are given in Table 1.

$$E = \sum_{i>j} f_C(r_{ij}) \left[V_R(r_{ij}) - \frac{b_{ij} + b_{ij}}{2} V_A(r_{ij}) \right] \tag{3a}$$

Table 1
Morse potential fitting parameters.

$D_0(eV)$	$\alpha\,(Å^{-1})$	$r_0(Å)$
0.002467	1.502	3.852

$$V_R(r) = \frac{D_0}{S-1}\, exp\left[-\beta\sqrt{2S}\,(r - r_0)\right],$$
$$V_A(r) = \frac{SD_0}{S-1}\, exp\left[-\beta\sqrt{\frac{2}{S}}(r - r_0)\right] \tag{3b}$$

The Morse Potential is given by:

$$E = D_0[exp[-2\alpha(r - r_0)] - 2exp[-\alpha(r - r_0)]] \tag{4}$$

3.2. Simulation details

The open-source Large-scale Atomic/Molecular Massively Parallel Simulator (LAMMPS) [34] package was used as the primary MD simulation engine. All three systems (i.e., FCC, T-phase and R-phase) were initially energy-minimized at 0 K using the Polak-Ribiere [35] version of the conjugate gradient algorithm, which served as the initial structure for equilibration at 300 K and 1 bar. Equilibration was achieved by subjecting the systems to isobaric-isothermal (NPT) and canonical (NVT) ensembles respectively for a total duration of 1 ns. MD simulations of the FCC phase used a timestep of 1 fs, while for the R-phase and the T-phases, the timestep was 0.1 fs. The size of the timestep was chosen to ensure energy conservation during NVE simulations, which were used for evaluating thermophysical properties.

To obtain specific heat at constant volume (C_V) and thermal conductivity (κ) at 300 K, each system was then subjected to an NVE ensemble for 10 ns, from which the velocity autocorrelation and thereby the vibrational density of states (DOS), as well as the heat current autocorrelation function (HCAF) were obtained. Note that under the classical harmonic approximation, the DOS is equivalent to the velocity autocorrelation power spectrum, and given by the Fourier transform of the velocity autocorrelation function.

Using the DOS ($g(\nu)$) and HCAF, C_V and κ can be obtained according to Eqns. (5) and (6).

$$C_v = \frac{h^2}{k_B T^2} \int_0^\infty \nu^2 g(\nu) \frac{e^{\left(\frac{h\nu}{k_B T}\right)}}{\left(e^{\left(\frac{h\nu}{k_B T}\right)} - 1\right)^2} d\nu \tag{5}$$

$$\kappa = \frac{V}{3k_B T^2} \int_0^\infty \langle J(0) \cdot J(t) \rangle dt \tag{6}$$

In Eqn. (6), which is based on the Green-Kubo formalism, V is the volume of the simulation cell, T is the temperature, k_B is the Boltzmann's constant and h is the Planck's constant. Further, the evaluation of J, which represents the heat current (given in Eqn. (7)), enables the calculation of the HCAF ($J(0)J(t)$). $J(t)$ is defined in terms of r_i, E_i, v_i, which represent the position, potential energy, velocity of the i^{th} atom respectively, while r_{ij} and F_{ij} represent the interatomic distance and force between the i^{th} and j^{th} atoms.

$$J = \frac{d}{dt} \sum_i r_i E_i = \sum_i E_i v_i + \sum_{i,j} (F_{ij} \cdot v_i) r_{ij} \tag{7}$$

To ensure convergence in the estimation of κ, a running average of J(t) was performed for the entire duration of the simulation(s) of 10 ns A careful study of the dependence of κ on the extent of the correlation time was carried out. It was seen that correlation times of 50 ps and 100 ps were required for the unpolymerized (FCC) and

polymerized phases (T- and R-phase) respectively. The integral in Eqn. (6) was evaluated using the trapezoidal rule. For each system, five different configurations, each with a different starting velocity distribution was used for providing statistical bounds on the estimated properties. A similar approach was undertaken to obtain the DOS and $\boldsymbol{C_V}$.

In addition to the 300 K equilibrated simulations, the 0 K energy minimized structures were subjected to uniform volume expansion and contraction (up to 5% deformation). For each volumetric deformation configuration (V), the structure was energy minimized (at constant volume) and the corresponding energy vs. volume (E-V) curves were obtained and used as the basis for obtaining $\boldsymbol{C_V}$, the Debye temperature ($\boldsymbol{\theta_D}$) and the coefficient of thermal expansion ($\boldsymbol{\alpha_T}$) as discussed below. The estimation of $\boldsymbol{C_V}$ independently from Eqn. (5) and the E-V curves, provide internally self-consistent validation of the adopted methods, while differences (if any) in the respective estimations can be used for understanding the contributions of the different degrees of freedom to $\boldsymbol{C_V}$.

The Birch-Murnaghan equation (Eqn. (8)) is invoked for fitting the E-V curves, with a, b, c, and d representing the fit parameters.

$$E(\boldsymbol{V}) = a + b\,\boldsymbol{V}^{-\frac{2}{3}} + c\,\boldsymbol{V}^{-\frac{4}{3}} + d\,\boldsymbol{V}^{-2} \tag{8}$$

The Debye temperature $\boldsymbol{\theta_D}$ within the Debye-Gruneisen approach can be calculated from the properties obtained from the ground state equation of state (EOS) and in general is defined as follows [36,37],

$$\theta_D(V) = sAV_0^{\frac{1}{6}}\left(\frac{B_0}{M}\right)^{\frac{1}{2}}\left(\frac{V_0}{V}\right)^{\gamma} \tag{9}$$

where $\boldsymbol{\gamma}$ is the Gruneisen constant describing the anharmonic effects of the vibrating crystal lattice and can be approximated either based on Slater [38] or Dugdale and Macdonald [39] expressions as given by $\gamma = \left[\frac{(1+B_0')}{2} - x\right]$. Here $\boldsymbol{x}$ is an adjustable parameter and is 2/3 for high temperatures (greater than $\boldsymbol{\theta_D}$) and 1 for low temperatures. In Eqn. (9), $\boldsymbol{A}$ is a constant equal to $(6\pi^2)^{\frac{1}{3}}\frac{h}{k_B} = 231.04$, $\boldsymbol{V}$ is volume/atom in Å^3, $\boldsymbol{B_0}$ is the bulk modulus in GPa and $\boldsymbol{M}$ is the atomic weight. $\boldsymbol{B_0}$, $\boldsymbol{B_0'}$ and $\boldsymbol{V_0}$ are obtained from an analysis of the curvature and minimum as obtained from Eqn. (8), while the reported Debye temperature $\boldsymbol{\theta_D}$ was evaluated for $V = V_0$. $\boldsymbol{s}$ is a scaling factor and is set to unity, based on a preliminary analysis for reproducing $\boldsymbol{\theta_D}$ for other carbon-based materials such as diamond and graphite.

$\mathbf{C_V}(\mathbf{T})$ and $\boldsymbol{\alpha_T}$, are evaluated from the Helmotz free energy $F(V,T)$ as follows;

$$F(V,T) = F_{vib}(V,T) + E(V)$$

$$F_{vib}(V,T) = \frac{9}{8}k_B\,\Theta_D(V) + k_BT\left\{3\ln\left[1-\exp\left(-\frac{\Theta_D}{T}\right)\right] - D\left(\frac{\Theta_D}{T}\right)\right\} \tag{10}$$

$$S = -\left(\frac{\partial F}{\partial T}\right)_V;\; C_V = T\left(\frac{\partial S}{\partial T}\right)_V;\; \alpha_V = \frac{1}{V_0^{300}}\left(\frac{dV}{dT}\right)_{V=V_o^{300}}$$

Finally, the 0 K energy minimized structures were also subjected to appropriate small strain deformations, to obtain the respective elastic stiffness tensors.

4. Results

As a first step towards characterizing the interplay between polymerization and the thermophysical properties, the accuracy of the developed potential was examined with respect to predicting the lattice parameters of the three systems under study. As evident from Table 2, the potential captures the effects of polymerization and correctly predicts the relative differences in the lattice parameters of the three phases; however, the lattice parameters are overestimated by ~4% for the FCC phase and by approximately 1% for the polymerized phases. For reference, the DFT-obtained structural properties of the FCC phase [29] is also given in Table 2.

Next, we turn our attention to the elastic moduli (Table 3); as expected, the extent of the polymerization leads to significant increase in the in-plane moduli ($\boldsymbol{C_{11}}$, $\boldsymbol{C_{22}}$); in particular, the covalent intermolecular bonds in the polymerized structures lead to an order of magnitude (~20X) change in the modulus; further, the R-phase demonstrates a higher modulus than the T-phase, a direct consequence of the increased extent of polymerization. Interestingly, despite restricting polymerization to being in-plane, both the T-phase and R-phase demonstrate an increase in the out-of-plane modulus ($\boldsymbol{C_{33}}$), which is correlated to a decrease in the out-of-plane inter-sheet separation. In particular, the formation of intermolecular covalent bonds leads to in-plane densification, which in turn allows a larger contribution from the van der Waal interactions between $\boldsymbol{C_{60}}$ molecules in the out-of-plane direction. On a related note, the increase in modulus is also reflected in the resulting increase in the longitudinal speed of sound ($\boldsymbol{v_s}$), which is related to the moduli as follows: $\boldsymbol{v_s} = \sqrt{\frac{\boldsymbol{C}}{\boldsymbol{\rho}}}$, where $\boldsymbol{\rho}$ is the mass density of the system.

The respective E-V curves for the three systems are given in Fig. 2. It is clear that the polymerized structures demonstrate higher curvatures (and therefore higher bulk modulus); more importantly, it is seen that despite applying uniform volume deformation (expansion or contraction), after energy minimization at every deformation step, the intramolecular bond distances remain virtually unchanged and the volume changes are only reflected as changes in the intermolecular and inter-sheet separation. Thus, the properties derived from the E-V curves correspond to those of the molecular solid, with the intramolecular and rotational degrees of freedom frozen out.

The thermophysical properties as derived from the E-V curves are given in Table 4. Of most interest is the variation in $\boldsymbol{\theta_D}$, as $\boldsymbol{\theta_D}$ represents the Debye limit for the unpolymerized (FCC) and polymerized (T-phase and R-phase) molecular solids, above which all

Table 2
Tabulation of the lattice parameters (a,c) and sheets separation distance of the of the FCC, T-phase and R-phase structures (Å). The experimental values are as reported in Refs. [40,41]. The calculated values as obtained in this work correspond to the energy-minimized structures at 0 K and structures at 300 K and 1 bar. The DFT calculations [29] for the FCC structure was based on a 4-molecule (~240 atoms) supercell and the corresponding 0 K lattice parameter is given in parenthesis. Note that the DFT calculation incorporated dispersion corrections, which are not accounted in standard local density approximation and generalized gradient approximation based functionals.

		Exp.	Energy Minimized (0 K)	At 300 K
FCC	a	14.04	14.42 (14.27)	14.61
T-phase	a	9.09	9.22	9.24
	c	14.95	15.16	15.2
	Sheet separation	7.48	7.67	7.56
R-phase	a	9.19	9.28	9.29
	c	24.50	24.74	24.78
	Sheet separation	8.17	8.31	8.25

Table 3
Elastic moduli (C_{11}, C_{22}, C_{33}, B_0) and the corresponding speeds of sound (V) of the FCC, T-phase and R-phase structures. Note that the in-plane properties are different than the out-of-plane properties for the polymerized phases.

	FCC	T-phase	R-phase
$C_{11}, C_{22} (GPa)$	11	201	228
$V_{11}^{sound}, V_{22}^{sound} \left(\frac{m}{s}\right)$	2717	10415	11141
$C_{33} (GPa)$	11	24	25
$V_{33}^{sound} \left(\frac{m}{s}\right)$	2717	3613	3726
$B_0 (GPa)$	8.2	59.9	76.3

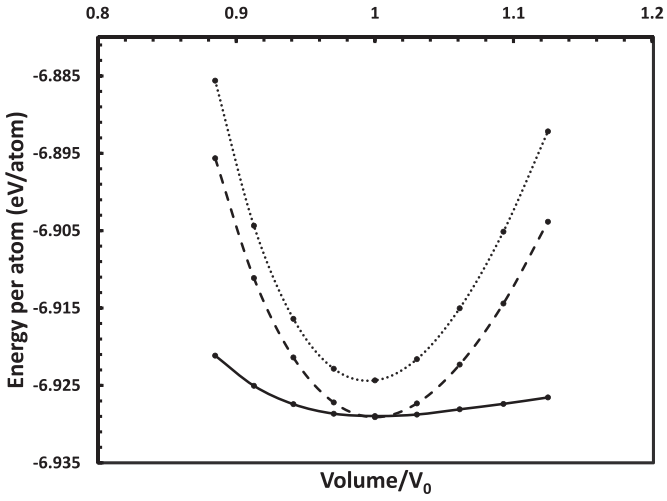

Fig. 2. Energy per atom vs. relative volume for the FCC (solid), T-Phase (dash) and R-Phase (dots) structures.

Table 4
Thermophysical properties volumetric thermal expansion (α_V), Debye temperature (θ_D), bulk modulus (B_0) and its derivative w.r.t pressure(B_0') of the FCC, T-phase and R-phase structures as obtained from the ground state equation of state (EOS).

	FCC	T-phase	R-phase
B_0	8.2	59.9	76.3
B_0'	15	4.6	5.4
Θ_D(K)	73	195	234
α_V (1/K) (10^{-6})	57.9	1.89	1.23

the intermolecular phonon modes are 'activated' and the molar specific heat (i.e., heat capacity of a mole of $\boldsymbol{C_{60}}$ molecules) reaches the Dulong-Petit limit (for molecular solids). Importantly, Table 4 shows that the absence of polymerization correlates to a lower $\boldsymbol{\theta_D}$ for the FCC phase, as compared to the polymerized phases. Of particular relevance is the fact even for the polymerized structures, $\boldsymbol{\theta_D}$ is less than room temperature (300 K). Further, the reported $\boldsymbol{\theta_D}$ for the FCC phase falls well within the bounds of the scatter in the reported literature values.

Other relevant observations include the fact that $\boldsymbol{\alpha_T}$ for the FCC phase is much larger (30–40 X) than that of the polymerized phases, indicating that at 300 K, the extent of anharmonicity is much more significant for the FCC phase.

To complement the predictions as obtained from the E-V curves, we now examine the DOS as estimated at 300 K for the three systems. The DOS explicitly captures both the temperature dependent intramolecular and intermolecular vibrations as well as contributions from the rotational degrees of freedom. For comparison, the DOS of an isolated $\boldsymbol{C_{60}}$ molecule is also given. Specifically, Fig. 3(a) and (b) depict the DOS for an isolated $\boldsymbol{C_{60}}$ molecule and the FCC solid respectively, while Fig. 4(a) and (b) provide the DOS of the T-phase and R-phase respectively.

For the isolated $\boldsymbol{C_{60}}$ molecule, only 46 out of the 174 vibrational degrees of freedom are distinct because of the high symmetry. These 46 molecular modes extend from 9 to about 60 THz as shown in Fig. 3(a) and are attributed to localized intramolecular $\boldsymbol{sp^2}$ modes. In the case of the FCC phase, there is a gap in the DOS between 2 and 9 THz. A comparison with the DOS of the isolated molecule clearly shows that the lower end of the spectrum (i.e., <2 THz) arises from the van der Waal intermolecular vibrations as well as molecular rotations. In contrast, for both T-phase and the R-phase, the band-gap characteristic of the FCC phase significantly shrinks, a direct consequence of the differences in the intermolecular bonding (i.e., van der Waal secondary bonding vs. covalent bonds). Interestingly, a similar shrinking of the band-gap was also reported by Renker et al. [42] who studied the effect of Rb-doping as well as the 1-D polymeric solid.

Using the DOS, $\boldsymbol{C_V}$ (in mJ/g/K) of the three phases were evaluated according to Eqn. (5) and the respective temperature dependence is shown in Fig. 5. We restrict our studies to 550 K, since it is known that the polymerized systems become unstable beyond 550 K [43,44]. The $\boldsymbol{C_V}$ of all three phases at 300 K contain additional rotational (only for FCC) and $\boldsymbol{sp^2}$ contributions, and are therefore larger than the E-V estimated values.

Next, using the DOS and E-V estimations in tandem, we isolated and identified the contributions of the different degrees of freedom (i.e., intramolecular vs. intermolecular vs. rotational) to the respective $\boldsymbol{C_V}$ at 300 K (Table 5). For the intermolecular contributions (derived from E-V), it is clear that the 3R limit is reached much before 300 K. Thus at 300 K, the intermolecular contributions correspond to 34.7 mJ/g/K for the three phases. Further, an analysis of the rotations of the $\boldsymbol{C_{60}}$ molecules in the FCC phase, showed that they were 'fully activated' at 300 K; thus the rotations provide another 17.3 mJ/g/K ($= \frac{3}{2}\boldsymbol{R/mol}$) for the FCC phase. Obviously, rotations are suppressed in the polymerized phases due to the covalent intermolecular bonding. Finally, the $\boldsymbol{sp^2}$ contributions were obtained by subtracting the above identified values from the total $\boldsymbol{C_V}$ estimated from the DOS. Comparisons with experiments demonstrate the ability to closely match experimental data [19,22].

In an effort to examine internal self-consistency, the contributions of the low frequency modes of the DOS to the specific heat were obtained by restricting the integral in Eqn. (5) to only these modes. Reassuringly, the specific heats of the low-frequency modes (0–2 THz) corresponding to the FCC phase, as well as that of the polymeric phases (~0–7 THz) were consistent with the respective intermolecular contributions as obtained from the E-V curves.

The next and final step towards characterizing the thermophysical properties involves the examination of the respective thermal conductivities κ In this regard, the thermal conductivity of the three systems as evaluated from MD is given in Table 6. Care was taken to accurately evaluate κ. Specifically, as seen in Fig. 6(a,b,c), the durations of the MD simulations were chosen to be sufficiently long to ensure convergence, and the reported κ values were averaged over the last three nanoseconds of each run. As evident from Table 6, the effect of polymerization results in a two order of magnitude increase in the in-plane thermal conductivity of both T-phase and the R-phase. Also, the out of plane thermal conductivities were an order of magnitude larger than unpolymerized FCC phase, similar to the increase in the out-of- plane moduli of the polymerized phases.

To understand the reasons underlying the significant increase in the in-plane thermal conductivity (κ_{11}, κ_{22}), we invoke the respective DOS. As discussed earlier, fundamental differences in the DOS exist between the unpolymerized and polymerized phases as seen by the presence of additional phonon modes between 2 and 7 THz,

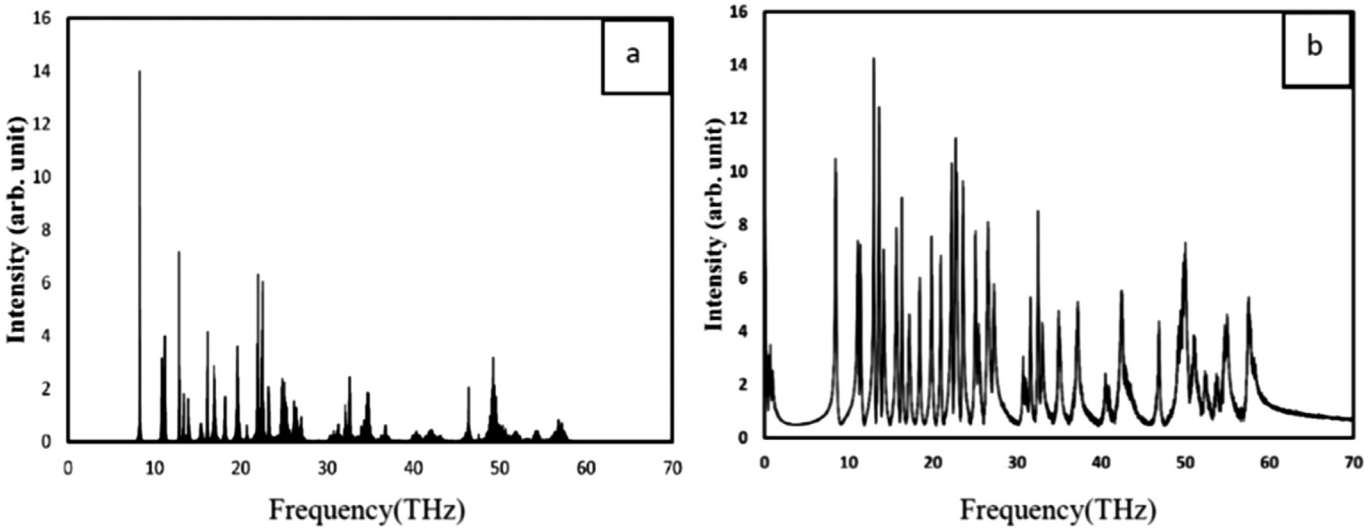

Fig. 3. DOS of (a) one C_{60} molecule and (b) C_{60} FCC crystal, up to the maximum supported frequency.

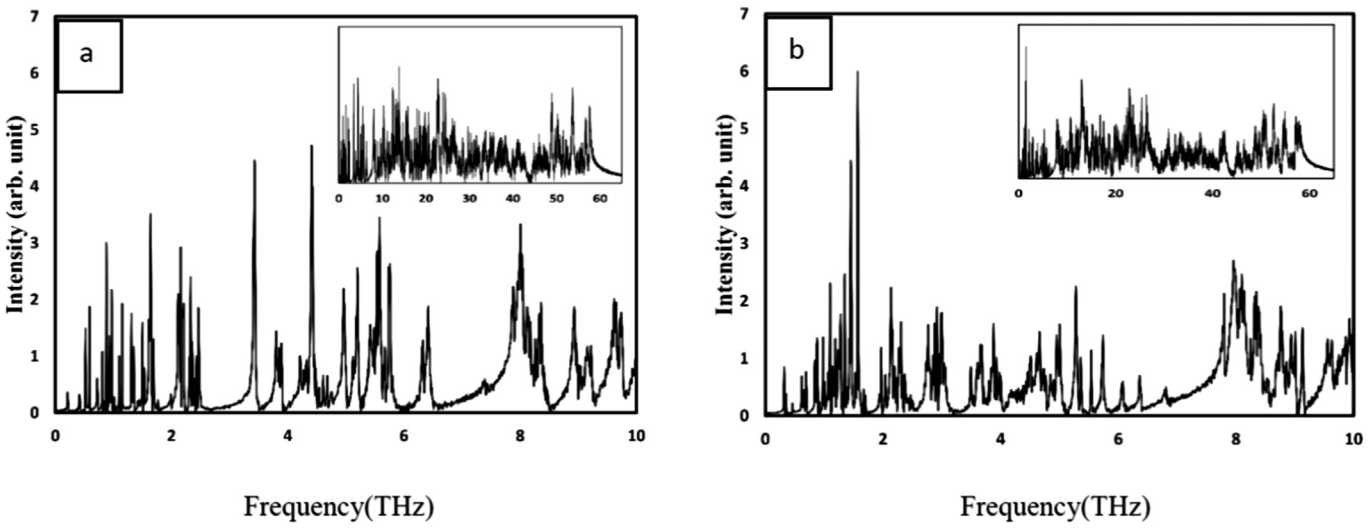

Fig. 4. DOS of (a) T-phase; (b) R-phase for the low frequency range (1–10 THz). The respective insets represent the total DOS up to the maximum supported frequency.

while the DOS look similar at other frequencies. Thus it can be discerned that the 'new' modes characteristic of the polymerized phases in the range 2–7 THz are the primary heat energy carriers, and these thermal phonons underlie the significant increase in the in-plane thermal conductivity of the polymerized phases. Further, in the FCC phase, only the low-frequency THz modes (<2 THz) can be considered as contributing towards thermal conductivity, since the higher frequency intramolecular modes ($\geq$***7 THz***) are localized within the C_{60} molecules.

Thus, it can be summarized that the frequencies between 2 and 7 THz that arise solely due to strong intermolecular bonds enable the significant increase in κ of the polymerized phases. The frequencies below 2 THz correspond to weaker van der Waal forces, which are the primary thermal phonon modes in the FCC phase. Frequencies greater than 9 THz arise due to sp^2 intramolecular interactions, but do not transport thermal energy in C_{60} solids. On a related note, using Eqn. (2) (which is a valid approximation at 300 K given the respective θ_D) in conjunction with v_s, C_V^ρ and κ, an effective mean free path (λ_p) of the thermal phonons were estimated for the three phases; it was seen that λ_p for the T-phase and R-phase was 5.9 nm and 7.5 nm, indicating that the coherence length of typical thermal phonons in the polymers extend across multiple covalently bonded C_{60} molecules. On the other hand, for the FCC phase, λ_p was approximately 0.3 nm.

While the focus of this study has been on 2-D polymerized C_{60} polymorphs, the observed inter-relationship between the extent of polymerization and the ensuing properties was applicable to the 1-D systems too. In particular, the mechanical modulus as well as the thermal conductivity of the O-phase, which consists of 1-D parallel chains of covalently bonded C_{60} molecules, were commensurate with the lower extent of polymerization associated with the O-phase. The bulk modulus and C_{11} of the O-phase (i.e. along the axis of polymerization) were 32 and 184 GPa respectively, which while lower than the 2- D counterparts, was still significantly higher than the FCC molecular solid. A similar trend was observed for the thermal conductivity of the O-phase along the polymerization axis (~5.6 W/m-K). Thus based on these observations, one can unambiguously state that the thermophysical properties of C_{60} solid-state polymorphs are directly dependent on the nature and extent of polymerization.

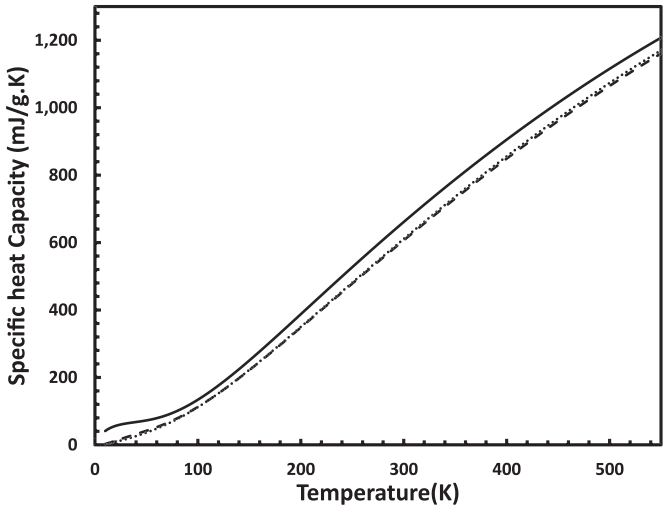

Fig. 5. Specific heat capacity (C_V) as a function of temperature as integrated from the DOS (Eqn. (5)) for the FCC (solid line), T-Phase (dash line) and R-Phase (dots line) structures.

Table 5
Intermolecular, intermolecular and rotational contributions to Heat capacity (C_v) (mJ/g.K) at 300 K of the FCC, T-phase and R-phase structures.

	FCC	T-phase	R-phase
Intramolecular	609.0	572.0	576.1
Intermolecular	34.7	34.7	34.7
rotation	17.3	NA	NA
Total	661.0	606.7	610.8

Table 6
Thermal conductivity (W/mK) at 300 K of the FCC, T-phase and R-phases respectively. For the FCC structure, the reported value was averaged over the three directions (x, y, z), while for the T-phase and R-phase the in-plane conductivity (k_{11} and k_{22}) was averaged over the x and y directions.

	FCC	T-phase	R-phase
k_{11}	0.26 ± 0.003	22.82 ± 0.33	32.9 ± 0.74
k_{22}	0.26 ± 0.003	22.82 ± 0.33	32.9 ± 0.74
k_{33}	0.26 ± 0.003	1.81 ± 0.07	7.66 ± 0.27

5. Conclusions and perspectives

In conclusion, using MD, we have rigorously examined the thermophysical properties of C_{60} molecular crystals. In particular, we have paid attention to the role of polymerization on the properties of 2-D polymerized $\boldsymbol{C_{60}}$ molecular solids. It is clearly seen that the formation of primary bonds between $\boldsymbol{C_{60}}$ molecules significantly enhances both mechanical and thermal properties. The 2-D polymerization of $\boldsymbol{C_{60}}$ introduces new delocalized THz phonon-modes that are chiefly responsible for heat conduction. The fact that there is a simultaneous orders of magnitude enhancements in both the thermal conductivity and mechanical modulus provides brand new avenues for adoption of $\boldsymbol{C_{60}}$ solids as acoustic and phononic metamaterials with on-demand tunable properties, enabling wide-ranging technologies for thermal and acoustics management. In particular, recent developments in obtaining reversibly polymerizable $\boldsymbol{C_{60}}$ structures [45], should enable the dynamic tunability of their vibrational properties, potentially leading to breaking of symmetry (e.g. time reversible symmetry). Thus, dynamically polymerizable $\boldsymbol{C_{60}}$ superlattices can be suitably utilized for designing unconventional devices such as thermal rectifiers, tunable surface acoustic wave filters and vibration dampeners. Such applications will be examined in a future study. In addition, similar studies that investigate polymerization driven tunability of functionalized $\boldsymbol{C_{60}}$ systems (e.g. PCBM in organic photovoltaics) will also be undertaken and strategies for developing multifunctional $\boldsymbol{C_{60}}$ based materials will be put forth.

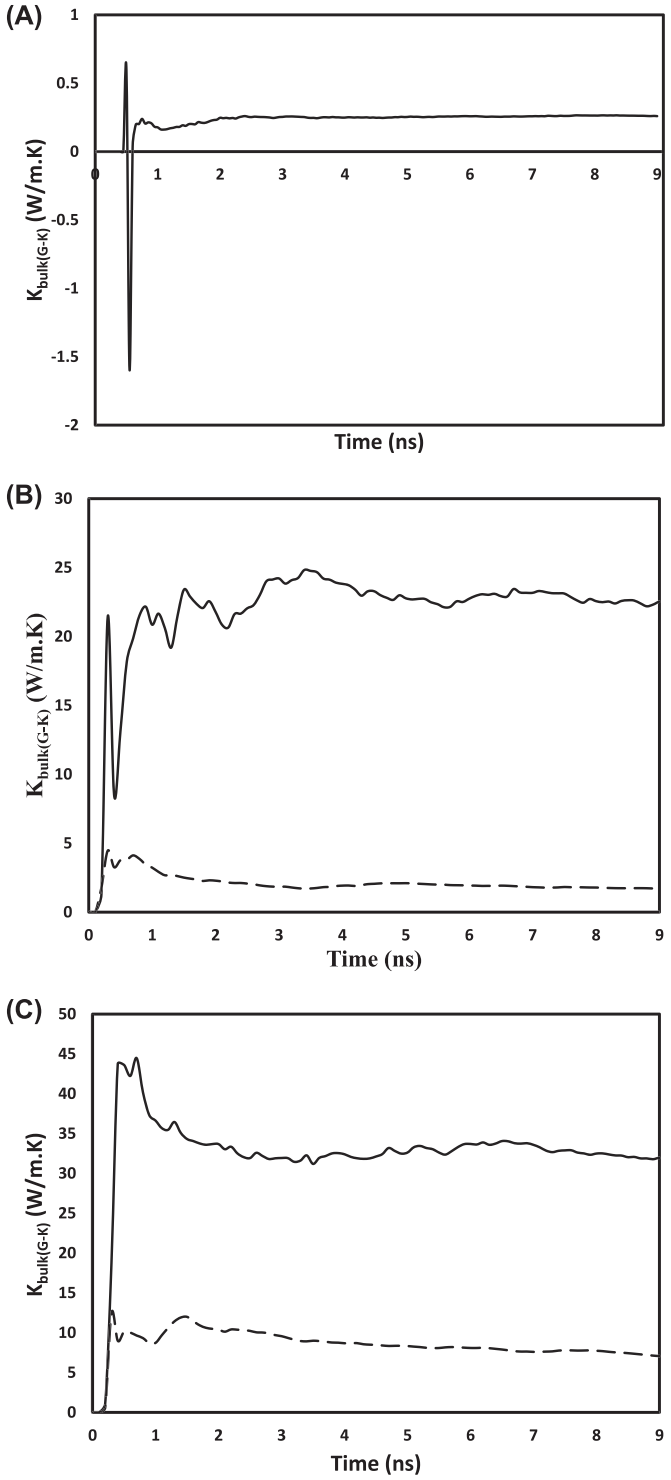

Fig. 6. Convergence of thermal conductivity as a function of time as calculated using Green-Kubo method of (a) C60 FCC crystal; (b) T-phase; (c) R-phase where the solid lines and the dashed lines represent the in-plane and out-of-plane thermal conductivities respectively.

Acknowledgment

The authors acknowledge Prof. Douglas Loy for useful discussions. The authors also gratefully acknowledge the University of Arizona High-Performance Computing (HPC) facility for the computing time allocated to this work. A.Q.A. acknowledges King Fahd University of Petroleum and Minerals for their financial support during his Ph.D.

References

[1] H.W. Kroto, J.R. Heath, S.C. O'Brien, R.F. Curl, R.E. Smalley, C 60: buckminsterfullerene, Nature 318 (1985) 162–163, https://doi.org/10.1038/318162a0.
[2] A.M. Rao, P. Zhou, K. a Wang, G.T. Hager, J.M. Holden, Y. Wang, W.T. Lee, X.X. Bi, P.C. Eklund, D.S. Cornett, M.A. Duncan, I.J. Amster, Photoinduced polymerization of solid C60 films, Science 259 (1993) 955–957, https://doi.org/10.1126/science.259.5097.955.
[3] V.A. Davydov, L.S. Kashevarova, A.V. Rakhmanina, V.M. Senyavin, Pressure-induced dimerization of fullerene C60: a kinetic study, Chem. Phys. Lett. 333 (2001) 224–229, https://doi.org/10.1016/S0009-2614(00)01379-8.
[4] K. Komatsu, K. Fujiwara, T. Tanaka, Y. Murata, Fullerene dimer C120 and related carbon allotropes, Carbon N. Y. 38 (2000) 1529–1534, https://doi.org/10.1016/S0008-6223(00)00051-8.
[5] G. Wang, K. Komatsu, Y. Murata, Synthesis and X-ray structure of dumb-bell-shaped C 120, Nature 387 (1997) 583–586, https://doi.org/10.1038/42439.
[6] T.J. Gnanaprakasa, D. Sridhar, W.J. Beck, K. Runge, B.G. Potter, T.J. Zega, P. a Deymier, S. Raghavan, K. Muralidharan, Graphene mediated self-assembly of fullerene nanorods, Chem. Commun. 51 (2015) 1858–1861, https://doi.org/10.1039/c4cc09362c.
[7] J.E. Fischer, P. a Heiney, a R. McGhie, W.J. Romanow, a M. Denenstein, J.P. McCauley, a B. Smith, Compressibility of solid c60, Science 252 (1991) 1288–1290, https://doi.org/10.1126/science.252.5010.1288.
[8] V.A. Davydov, L.S. Kashevarova, A.V. Rakhmanina, V.M. Senyavin, R. Céolin, H. Szwarc, H. Allouchi, V. Agafonov, Spectroscopic study of pressure-polymerized phases of C 60, Phys. Rev. B 61 (2000) 11936–11945, https://doi.org/10.1103/PhysRevB.61.11936.
[9] A.J.H. McGaughey, M. Kaviany, Quantitative validation of the Boltzmann transport equation phonon thermal conductivity model under the single-mode relaxation time approximation, Phys. Rev. B 69 (2004) 94303, https://doi.org/10.1103/PhysRevB.69.094303.
[10] C. Kittel, Introduction to Solid State Physics, John wiley & sons, inc, 1953.
[11] R. Bini, P. Procacci, P.R. Salvi, V. Schettino, The far-infrared spectrum of crystalline fullerene C60, J. Phys. Chem. 97 (1993) 10580–10584, https://doi.org/10.1021/j100143a011.
[12] R. Heid, L. Pintschovius, J.M. Godard, Eigenvectors of internal vibrations of C60: theory and experiment, Phys. Rev. B 56 (1997) 5925–5936, https://doi.org/10.1103/PhysRevB.56.5925.
[13] L. Pintschovius, S.L. Chaplot, Neutron scattering study of the intermolecular vibrations in solid C60, Z. Phys. B Condens. Matter 98 (1995) 527–540, https://doi.org/10.1007/BF01320854.
[14] M. Matus, H. Kuzmany, Raman spectra of single-crystal C60, Appl. Phys. A Solids Surfaces 56 (1993) 241–248, https://doi.org/10.1007/BF00539482.
[15] S. Rols, J. Cambedouzou, J.L. Bantignies, F. Rachdi, J.L. Sauvajol, V. Agafonov, A.V. Rakhmanina, V.A. Davydov, B. Hennion, R. Kahn, Lattice dynamics of pressure-polymerized phases of C60: a neutron scattering investigation, Phys. Rev. B Condens. Matter 70 (2004) 1–6, https://doi.org/10.1103/PhysRevB.70.104302.
[16] R.C. Yu, N. Tea, M.B. Salamon, D. Lorents, R. Malhotra, Thermal conductivity of single crystal C60, Phys. Rev. Lett. 68 (1992) 2050–2053, https://doi.org/10.1103/PhysRevLett.68.2050.
[17] A.F. Hebard, Superconductivity in doped fullerenes, Phys. Today 45 (1992) 26–32, https://doi.org/10.1063/1.881320.
[18] B. Wunderlich, Y. Jin, The thermal properties of four allotropes of carbon, Thermochim. Acta 226 (1993) 169–176, https://doi.org/10.1016/0040-6031(93)80218-Y.
[19] M.I. Bagatskii, V.V. Sumarokov, M.S. Barabashko, A.V. Dolbin, B. Sundqvist, The low- temperature heat capacity of fullerite C60, Low Temp. Phys. 41 (2015) 630–636, https://doi.org/10.1063/1.4928920.
[20] A. Inaba, T. Matsuo, Lattice vibrations and thermodynamic stability of polymerized C 60 deduced from heat capacities, Chem. Phys. 110 (1999) 12226–12232, https://doi.org/10.1063/1.479160.
[21] C. Guang-Lei, G. Min, Y. Yao, X. Xi-Bin, W. Li-Hang, C. Xiao, F. Duan, T.T. Bor, Specific heat of rhombohedral polymeric C 60 in temperature range 300 – 2 K, Chin. Phys. Lett. 25 (2008) 1–4.
[22] A.V. Markin, N.N. Smirnova, B.V. Lebedev, A.G. Lyapin, V.V. Brazhkin, Thermodynamics of 2D polymerized tetragonal phase of fullerene C 60 in the range from T → 0 to 650 K at standard pressure, Thermochim. Acta 411 (2004) 101–108, https://doi.org/10.1016/j.tca.2003.08.004.
[23] B.V. Lebedev, A.V. Markin, Thermodynamic Properties of C 60 polyfullerites, Phys. Solid State 44 (2002) 434–436, https://doi.org/10.1134/1.1462664.
[24] A.V. Markin, N.N. Smirnova, B.V. Lebedev, V.A. Davydov, L.S. Kashevarova, A.V. Rakhmanina, Thermodynamic properties of crystalline polymeric C60 phases in the temperature region from T → 0 to 340 K, Russ. Chem. Bull. 52 (2003) 862–868, https://doi.org/10.1023/A:1024487923259.
[25] A. Soldatov, O. Andersson, B. Sundqvist, K. Prassides, Transport and vibrational properties of pressure polymerized C 60, Mol. Mater. 11 (1998) 1–6.
[26] A. Soldatov, O. Andersson, Thermal conductivity of pressure polymerized C60, Appl. Phys. A 64 (1997) 227–229, https://doi.org/10.1007/s003390050471.
[27] P. a. Persson, O. Andersson, P. Jacobsson, A. Soldatov, B. Sundqvist, T. Wagberg, The physical properties of high-pressure polymerized C60, J. Phys. Chem. Solid. 58 (1997) 1881–1885, https://doi.org/10.1016/S0022-3697(97)00086-3.
[28] O. Andersson, A. Soldatov, B. Sundqvist, Thermal conductivity of C60 at pressures up to 1 GPa and temperatures in the 50–300 K range, Phys. Rev. B 54 (1996) 3093–3100, https://doi.org/10.1103/PhysRevB.54.3093.
[29] S. Jalali-Asadabadi, E. Ghasemikhah, T. Ouahrani, B. Nourozi, M. Bayat-Bayatani, S. Javanbakht, H.A. Rahanamaye-Aliabad, I. Ahmad, J. Nematollahi, M. Yazdani-Kachoei, Electronic structure of crystalline buckyballs: FCC-C60, J. Electron. Mater. 45 (1) (2016) 339–348.
[30] L. Malakkal, B. Szpunar, R.K. Siripurapu, J.A. Szpunar, Thermal conductivity of buk and nanowire cubic-SiC from ab initio calculations, Comput. Mater. Sci. 128 (2017) 249–256.
[31] P. Erhart, K. Albe, Analytical potential for atomistic simulations of silicon, carbon, and silicon carbide, Phys. Rev. B Condens. Matter 71 (2005) 1–14, https://doi.org/10.1103/PhysRevB.71.035211.
[32] T.C. O'Connor, J. Andzelm, M.O. Robbins, AIREBO-M: a reactive model for hydrocarbons at extreme pressures, J. Chem. Phys. 142 (2015), https://doi.org/10.1063/1.4905549.
[33] J.H. Los, A. Fasolino, Intrinsic long-range bond-order potential for carbon: performance in Monte Carlo simulations of graphitization, Phys. Rev. B 68 (2003) 24107, https://doi.org/10.1103/PhysRevB.68.024107.
[34] S. Plimpton, Fast parallel algorithms for short – range molecular dynamics, J. Comput. Phys. 117 (1995) 1–19, https://doi.org/10.1006/jcph.1995.1039.
[35] E. Polak, G.R. Note, Note sur la convergence de méthodes de directions conjuguées, Rev. Fr. D'inf. Rech. Opérationnelle. Sé- Rie Rouge, Tome 3 (1969) 35–43.
[36] F. Birch, Finite elastic strain of cubic crystals, Phys. Rev. 71 (1947) 809–824, https://doi.org/10.1103/PhysRev.71.809.
[37] F. Birch, Finite strain isotherm and velocities for single-crystal and polycrystalline NaCl at high pressures and 300K, J. Geophys. Res. 83 (1978) 1257–1268, https://doi.org/10.1029/JB083iB03p01257.
[38] J.C. Slater, Introduction to Chemical Physics, McGraw-Hill, Newyork, 1939.
[39] J.S. Dugdale, K.C. MacDonald, The thermal expansion of solids 89 (1953) 832–834, https://doi.org/10.1103/PhysRev.89.832.
[40] R.M.I. William, I.F. David, K.P. Judy, C. Matthewman, T.J.S. Dennis, J.P. Hare, H.W. Kroto, R. Taylor, D.R.M. Walton, Crystal structure and bonding of ordered C60, Lett. Nat. 353 (1991) 737–740, https://doi.org/10.1038/353147a0.
[41] M. Núñez-Regueiro, L. Marques, J.L. Hodeau, O. Béthoux, M. Perroux, Polymerized fullerite structures, Phys. Rev. Lett. 74 (1995) 278–281, https://doi.org/10.1103/PhysRevLett.74.278.
[42] B. Renker, H. Schober, R. Heid, P. Stein, Pressure and charge induced polymerisation of C60: a comparative study of lattice vibrations, Solid State Commun. 104 (1997) 7–10, https://doi.org/10.1016/S0038-1098(97)00375-X.
[43] P. Nagel, V. Pasler, S. Lebedkin, A. Soldatov, C. Meingast, B. Sundqvist, P.A. Persson, T. Tanaka, K.B.S.I.A. Komatsu, C-60 one- and two-dimensional polymers, dimers, and hard fullerite: thermal expansion, anharmonicity, and kinetics of depolymerization, Phys. Rev. B 60 (1999) 16920–16927, https://doi.org/10.1103/PhysRevB.60.16920.
[44] Y. Iwasa, K. Tanoue, T. Mitani, T. Yagi, Energetics of polymerized fullerites, Phys. Rev. B Condens. Matter 58 (1998) 16374–16377, https://doi.org/10.1103/PhysRevB.58.16374.
[45] M. Nakaya, M. Aono, T. Nakayama, Molecular-scale size tuning of covalently bound assembly of C60 molecules, ACS Nano 5 (2011) 7830–7837, https://doi.org/10.1021/nn201869g.